Polymer 49 (2008) 5533–5540

Contents lists available at ScienceDirect

Polymer

journal homepage: www.elsevier.com/locate/polymer

Morphology development in photopolymerization-induced phase separated mixtures of UV-curable thiol-ene adhesive and low molecular weight solvents

Andrew J. Guenthner*, David M. Hess, Jessica J. Cash

Naval Air Warfare Center, Weapons Division, China Lake, CA 93555, United States

ARTICLE INFO

Article history:
Received 11 June 2008
Received in revised form 22 September 2008
Accepted 3 October 2008
Available online 17 October 2008

Keywords:
Photopolymerization-induced phase separation
Thiol-ene
Morphology

ABSTRACT

The influence of photopolymerization rate, solvent quality, and processing parameters on the photopolymerization-induced phase separated morphology of mixtures of thiol-ene based optical adhesive with mixed solvents of diglyme and water or acetone and isopropanol is described. Upon exposure to UV radiation (~50 mW/cm^2, 365 nm) for periods of 10–90 s, homogeneous solutions of 5–10 wt% NOA65 and NOA81 adhesive formed phase separated structures with characteristic sizes ranging from 400 nm to 10 μm, with increased photopolymerization rates leading to smaller feature sizes. In the systems containing diglyme and water, morphologies formed by phase separation at a lower degree of photopolymerization were characteristic of spinodal decomposition, while morphologies formed by phase separation at a higher degree of photopolymerization exhibited characteristics of viscoelastic phase separation. In the systems containing acetone and isopropanol, interactions between evaporation and photopolymerization-induced phase separation led to the development of more complicated morphologies, including three-dimensional sparse networks. These morphologies provide a combination of connectivity and low overall volume fraction that can significantly enhance the performance of many multi-functional structures.

Published by Elsevier Ltd.

1. Introduction

Controlled phase separation in polymer solutions has long been used as an effective means of creating useful polymer products based on well-defined morphological features. Examples include scaffolds for biological tissues [1], absorbent fibers [2], liquid crystal displays [3], foams [4], and microporous carbon [5]. Both thermally induced phase separation [6] and reaction-induced phase separation [7,8] have been used in the applications cited above. For large-scale production, reaction-induced phase separation based on UV photochemistry (photopolymerization-induced phase separation, or PIPS) is often attractive because (1) it is conveniently scaled to large size; (2) structure formation can be accomplished in a short time, thus it is readily incorporated into continuous production processes; and (3) the incorporation of macro-scale patterning is achieved with simple and reliable masking techniques.

An additional advantage of thermosetting PIPS processes is that they readily form structures with a sub-micron feature size [9]. As the increase in polymer molecular weight drives the system towards increasing instability with respect to composition over time, rapid polymerization can result in virtual immobility of the polymer chains before coarsening processes have time to take effect. Structures formed by PIPS thus can retain many of the characteristics of patterns formed in the early stages of spinodal decomposition, such as a uniform feature size and a high degree of connectivity [10]. As an additional benefit, the cross-linked nature of the polymers formed during thermosetting PIPS typically imparts sufficient durability for the structures to survive subsequent handling and processing without being damaged.

In recent years, many of the effects observed in PIPS have been systematically explained using viscoelastic phase separation theory, which takes into account the drastic differences in the mobility of the separating phases [11–14]. As a result, the range of polymer morphologies that may be produced "on demand" (via scientific investigation followed by selection of the appropriate production process) has been extended to include, for example, very small droplets and sparse networks (interconnected morphologies formed by a component at low volume fractions). To date, though, the exploitation of viscoelastic phase separation to form such morphologies [15] has been limited.

If viscoelastic phase separation can be exploited to form polymer structures such as micro-droplets or sparse networks via a thermosetting PIPS processes, then the advantages for large-scale production inherent in PIPS will become available for affordably creating a wider range of useful morphologies. In fact, the formation of sparse network morphologies using thermosetting PIPS has

* Corresponding author. Tel.: +1 760 939 1626; fax: +1 760 939 1617.
E-mail address: andrew.guenthner@navy.mil (A.J. Guenthner).

0032-3861/$ – see front matter Published by Elsevier Ltd.
doi:10.1016/j.polymer.2008.10.005

already been noted on occasion in the context of forming polymer dispersed liquid crystals, even though in those cases it was not studied extensively since it was not the primary focus of the work [16–18]. However, for larger scale industrial applications, materials that are less expensive than liquid crystals need to be investigated. Potential applications for these controlled polymer microstructures include separation media, super-absorbents, and temperature-insensitive electrically conductive structures employing a sparse network of conductive polymer.

In what follows we describe how we utilized the principles of viscoelastic phase separation to create well-defined polymer microspheres and three-dimensional interconnected networks through a PIPS process using solutions of photopolymerizable thiol-ene adhesives. We investigated the effect of process variables such as polymerization rate, adhesive/solvent interaction energy, and solvent boiling point on the final morphology obtained by UV cure-induced phase separation. We found a number of simple and easily scalable techniques for controlling the size, interconnectedness, and three-dimensionality of the structures formed. The results may be readily extended to other material systems, demonstrating the potential of PIPS as an effective process for generating well-defined polymer microstructures in a wide variety of applications.

2. Experimental

Our general experimental procedure consisted of undertaking UV photopolymerization-induced phase separation under ambient conditions (22 ± 1°C, 30 ± 5% relative humidity) on solutions of commercially available thiol-ene optical adhesive formulations. The photopolymerization kinetics of thiol-enes has been previously studied [19–22] and the adhesives have been frequently employed in PIPS experiments [16,17,23]. The effect of polymerization rate was examined by employing two different commercial grades of the optical adhesive. The effect of adhesive/solvent interaction was studied by systematically varying co-solvent ratios. Lastly, comparisons were made between PIPS experiments carried out using high and low boiling solvent mixtures.

2.1. Materials

Norland® optical adhesives (products NOA81, which cures rapidly, and NOA65, which cures more slowly) were obtained from Norland Products (Cranbury, NJ) and used as-received. NOA65 has been reported as containing a mixture of trimethylopropane diallyl ether, trimethyopropane tristhiol, and isophorone diisocyanate ester, with a benzophenone photoiniator [23–25]. Polyethylene glycol (PEG) (average molecular weight ~4000), isopropanol, 2-methoxyethyl ether (diglyme, m.w. = 134), and acetone were purchased from Aldrich (histological grade, 99.5% pure) and used as-received. De-ionized water (~4.0 MΩ) was provided from an in-house source.

2.2. Fabrication with high-boiling point solvents

A total of 100 mg of either thiol-ene mixture were weighed out in 20 mL glass sample vials at room temperature. The adhesive dissolved quickly with the addition of 1.3–1.6 g diglyme. De-ionized water was then slowly added to the solution over approximately 2 min to make a final composition of 5.5 wt% adhesive with diglyme/water ratios of 3:1, 4:1, 5:1, and 8:1 by weight. Rapid addition of water was avoided in order to prevent precipitation of the adhesive. The stability and homogeneity of these solutions were further verified by cooling small samples of each until precipitation was observed, then returning them to room temperature. In all cases, the precipitate re-dissolved completely and no signs of inhomogeneity were seen on standing for several days. In addition, cloud points for various solution compositions were obtained with the aid of a Cincinnati Sub-Zero Micro-Climate chamber using heating and cooling rates of 0.1 °C/min.

Solutions freshly prepared and maintained at room temperature were blade cast onto clean glass microscope slides to form ~180 μm thick films. After coating, samples were exposed to ~50 mW/cm^2 365 nm UV light from a Norland Opticure 4 UV Curing Unit with the emitter fixed in place 1 cm above the sample for 60 s for NOA81 and 300 s for NOA65. In all cases, a translucent white precipitate formed and the formation times were noted. The films were then allowed to dry at ambient conditions.

2.3. Fabrication with low boiling solvents

A 2.5 wt% polyethylene glycol in acetone solution was formed through sonication. A total of 100 mg of NOA81 were then dissolved using 150–400 mg of isopropanol, followed by the addition of 500–750 mg of PEG/acetone solution over approximately 2 min so as not to induce product precipitation. The final concentration of NOA81 was 10.0 wt%.

As with the high-boiling solvents, the solutions were blade cast onto glass microscope slides to form ~180 μm thick films and exposed to ~50 mW/cm^2 365 nm UV light for 60 s, with the times required for the onset of phase separation noted. The samples were then heated on a digitally monitored hot plate at 100 °C in ambient air for 1.25 min, and allowed to cool gradually. Once cooled to room temperature the samples were submerged in a de-ionized water (ambient temperature) bath for 5 min to selectively dissolve the PEG while maintaining the structure formed by the NOA81.

2.4. Characterization

Atomic force microscopy (AFM) was performed on a Veeco Digital Instruments 3100 with a Nanoscope 3A controller. Fourier Transform-Infrared Spectroscopy (FT-IR) was performed on a Nexus 870 series FT-IR spectrometer in ATR mode. A Spectratech Foundation Series Thunderdome ATR adapter was used in conjunction with the Nexus operating system. Scanning electron microscopy (SEM) was performed with a Zeiss EVO-50 30 kV maximum accelerating voltage scanning electron microscope. Samples were observed at a maximum of 20 kV accelerating voltage under high vacuum with a variable pressure detector.

3. Results and discussion

3.1. PIPS in mixtures of thiol-ene and high-boiling solvents

In addition to the phase behavior, key variables that can influence morphology development during PIPS include the chemical composition, temperature, and UV radiation intensity. A check of the evaporation rates of diglyme and water in our laboratory found that within the time frame and geometrical parameters of the experiments, the change in composition due to evaporation was negligible. The high clarity and low thickness of the wet films used in our investigation helped to ensure that a significant gradient in intensity did not exist through the film thickness. Because of the slow rates of evaporation, temperature gradients caused by evaporative cooling were also judged negligible. Therefore, under the conditions used for our investigation, the photopolymerization rate and the initial system composition in relation to the phase diagram were expected to be the main factors controlling the development of morphology.

3.1.1. Phase behavior

A valuable and widely used starting point for understanding the development of morphology via phase separation is the determination of the system phase diagram prior to photopolymerization. However, for the systems under investigation, an experimental determination of the phase behavior is limited to a narrow temperature range because the Norland Optical Adhesives were found to vitrify at about −10 °C and to undergo thermal polymerization at temperatures above 55 °C. These effects resulted in behavior that was not completely thermally reversible using heating rates as low as 0.1 °C/min. These effects precluded performing the traditional thermal quench experiments at compositions near the critical point, since they would have necessarily involved exposure to temperatures much higher than the upper limit for fully thermally reversible behavior. We did, however, perform thermal quench experiments at very low and high concentrations of adhesive where cloud point data was also obtained. As expected, these showed formation of 10–100 μm domains of the minority component in widely varying sizes. We observed no phase separation among the individual components of the Norland Optical Adhesives over the temperature range investigated.

Due to the limited range of experimental data available, we explored the use of thermodynamic models to provide additional information about the expected phase behavior. As with many material systems in established industrial use, the utilization of thermodynamic models presents many challenges, owing to the complex mixture of chemical species present and the limited amount of available component thermodynamic data. Thus, our aim in developing the models was simply to help evaluate our qualitative interpretations of the experimental data rather than to make quantitative predictions about system behavior.

We investigated a number of crude thermodynamic models for our (generally speaking, oligomeric) system, based on either the Flory–Huggins theory [26,27], which is widely used for polymers, or the UNIFAC (Dortmund) approach [28], which is more appropriate for simple, small molecules. We investigated both pseudo-ternary (considering the adhesive as a single component) and pseudo-binary (considering both adhesive and solvent as separate single components) versions. For the Flory–Huggins approach, we estimated the interaction parameters using the published Hildebrand solubility parameters of diglyme and water [29], and the calculated solubility parameters based on correlations by Bicerano [30] for a model adhesive containing a 2:2:1 molar mixture of the diallyl ether, tristhiol, and diisocyante ester components of NOA65. For the UNIFAC (Dortmund) model, we used the same model adhesive composition, which allows the published interaction parameters to cover more than 90% of the group combinations present in a typical mixture. For the remaining group combinations, the missing interaction parameters were filled in using the available values for the most similar group (CH_2S or CS_2 for CH_2SH and CH_2S, or CH_3OH for H_2O and CH_2O). Despite the need for these approximations to complete the UNIFAC (Dortmund) model, it retains the significant advantage of describing strongly polar and hydrogen-bonding type interactions, unlike the Hildebrand/Flory–Huggins approach.

The phase equilibrium points for all models were computed by iteratively balancing the chemical potential of each model component in all phases, using a commercially available Generalized Reduced Gradient nonlinear optimization code. Note that technically these models do not contain any adjustable parameters, however, the many choices examined as part of their implementation constitute the *de facto* use of adjustable parameters.

Fig. 1 shows visually observed cloud point data for a mixture of NOA81 with 75 wt% diglyme and 25 wt% water, along with predicted values from the pseudo-binary versions of the UNIFAC

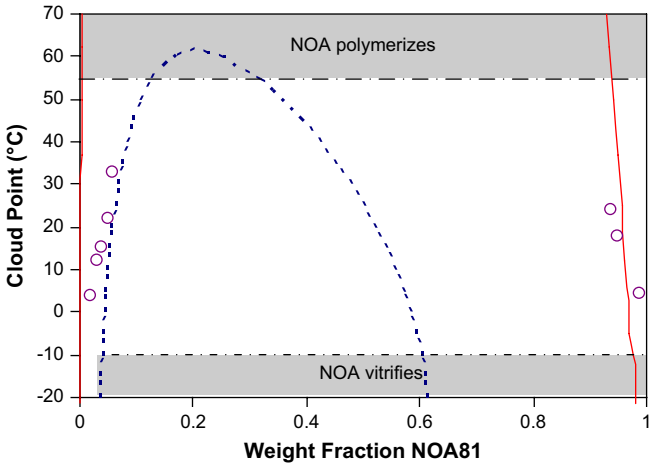

Fig. 1. Phase diagram of pseudo-binary mixture of NOA81 in a solvent comprised of 75 wt% diglyme and 25 wt% water. NOA81 experimental data (open circles), pseudo-binary UNIFAC (Dortmund) model (dashed line), and pseudo-binary Flory–Huggins model (solid line).

(Dortmund) and Flory–Huggins models, plotted as a function of the NOA81 weight fraction (that is, the weight of NOA81 divided by the total weight in the initially prepared solution prior to casting). The UNIFAC (Dortmund) model provided the best qualitative prediction of the experimentally observed solubility of the adhesive in the solvent, while the Flory–Huggins model provided the better qualitative prediction of the experimentally observed solubility of the solvent in the adhesive. Both models predicted an upper critical solution temperature (UCST) type phase diagram, a feature that was consistent with the experimental data. The pseudo-ternary versions of these models predicted very low solubility for the optical adhesive and failed to predict the complete miscibility of water and diglyme. Experimentally, water and diglyme exhibit a strongly negative heat of mixing [31], which is a better match to the assumption underlying the pseudo-binary models.

Fig. 2 shows the cloud point for mixtures of 5 wt% NOA65 and NOA81 as a function of the proportion (by weight) of water to the total amount of water and diglyme in the system, compared with the predictions of the pseudo-binary UNIFAC (Dortmund) and Flory–Huggins modes. Both models greatly overestimated the dependence of cloud point on water content, but did indicate that

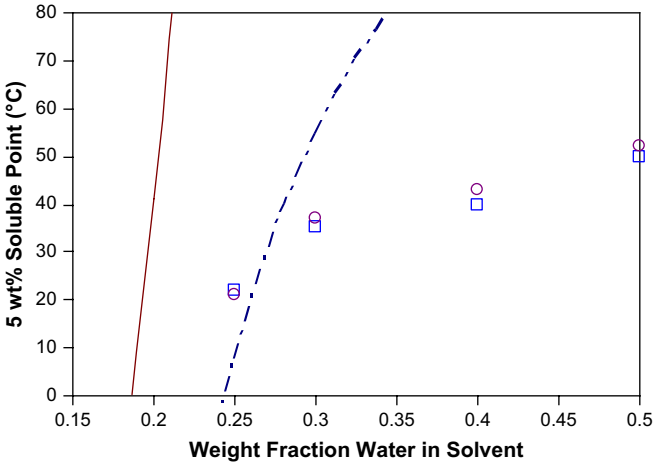

Fig. 2. Cloud point of mixtures containing 5 wt% NOA81 and NOA65 in water/diglyme as a function of water content. NOA81 experimental data (open circles), NOA65 experimental data (open squares), pseudo-binary UNIFAC (Dortmund) model (dashed line), and pseudo-binary Flory–Huggins model (solid line).

adding water to the system would increase the cloud point, a trend also clearly seen in the experimental data. It is also important to note that the experimentally observed cloud points for NOA65 and NOA81 were very similar, thus for our purposes the primary difference between NOA65 and NOA81 was in the rate of polymerization rather than in phase behavior.

Although no single model was able to even qualitatively match all of the experimental data, the predicted model trends support the interpretation of the experimental data that the system exhibits UCST type behavior (with the critical temperature well above ambient), and that the higher the water content in the system, the more the phase diagram is shifted to higher temperatures.

3.1.2. Morphology development due to UV irradiation

Exposure to UV radiation had a dramatic effect on phase separation and morphology development in the thin sheets of NOA81 and NOA65 solutions that we observed. Although solvent evaporation eventually pushed the systems into the two-phase region of the phase diagram, when no UV radiation was present the process took anywhere from several minutes to many hours, and always produced 10–100 μm droplets of adhesive in highly variable sizes that were typically not uniformly distributed across the sheets and varied considerably from one experiment to the next. In sharp contrast, when the sheets were exposed to UV radiation, a very fine (~1 μm particle size or less) morphology appeared at times ranging from 10 to 90 s. These morphologies were highly uniform across the exposed areas and showed no discernable variations when experiments were repeated. Thus the effects of photopolymerization were clearly distinguished from those due to evaporation or temperature change.

Our observations revealed that NOA81 cures at about four times the rate of NOA65, thus NOA81 was the focus of our investigation. The observed times for full cure (1–4 min) were in rough agreement with the manufacturer's specification and were determined by monitoring via FT-IR the disappearance of the thiol band at 2570 cm^{-1}. The actual kinetics of cure can be quite complicated during phase separation, owing to concentration changes and fluctuations in UV radiation. Qualitatively, though, after a very brief induction period the molecular weight of the adhesives will increase under UV irradiation until maximum conversion is achieved [20].

During photopolymerization of systems with an UCST, the bimodal and spinodal lines in the phase diagram shift to higher temperatures and lower polymer concentrations, being driven by the increase in molecular weight of the polymer [7]. As a result, initially homogeneous mixtures will pass through the metastable region of the phase diagram and enter the unstable region. Because the process occurs over a timescale of seconds, the passage through the metastable region should have a very limited effect on the structure formed. Thus, in the absence of viscoelastic effects, the structures formed will most likely be dominated by the process of spinodal decomposition. Since the systems under investigation contain only about 5% optical adhesive by volume, such a structure would be expected to feature polymer droplets of a relatively uniform size, the growth of which could be arrested at an early stage by vitrification of the photocured material.

In addition to creating phase instability, the polymerization also rapidly increases the dynamic asymmetry of the system over time, with molecules of the solvent being able to diffuse much faster than the cross-linked optical adhesive, but with the vast majority of mechanical stress in the system being borne by the developing polymer network. These effects could result in morphologies dominated by the effects of viscoelastic phase separation rather than spinodal decomposition. In particular, in a system with a low volume fraction of high molecular weight polymer, viscoelastic phase separation is expected to produce a web-like structure [32].

The morphological patterns dominated by spinodal decomposition (beads) and by viscoelastic phase separation (web) are quite different, suggesting that a wide range of morphologies may be obtained from photocured adhesive/solvent mixtures if the relative influence of viscoelastic phase separation can be varied. In fact, Fig. 3, which shows SEM images of photocured NOA81 mixed with water and diglyme in varying ratios, illustrates that such variations exist and are easy to control by adjusting the co-solvent composition. In Table 1, the compositions used to generate the samples imaged in Figs. 3a–d are listed, along with the time of UV irradiation required to achieve visible phase separation. As the amount of water in the system is increased, the phase separation occurs after a shorter time interval, even though the cure kinetics in the homogeneous layer of NOA81 should be quite similar. This result is easily explained by noting that with more water in the system, the cloud point increases, bringing the system closer to the two-phase region initially (see Fig. 2). Thus, a lower extent of polymerization is needed to shift the phase diagram sufficiently for the system to enter the unstable region. Consequently, by increasing the amount of water in the system, the onset of phase separation takes place when the molecular weight (and thus the dynamic asymmetry) is lower, meaning that viscoelastic effects are less important.

The differences in morphology can be substantial, as Fig. 3 illustrates. With a diglyme to water ratio of 8:1 by weight (Fig. 3a), the only evidence of phase separation is the presence of "craters" in the NOA81 film. These presumably result from pockets of solvent that form via viscoelastic phase separation and subsequently collapse during solvent evaporation. At 5:1 diglyme to water in the solvent mixture (Fig. 3b), the resulting structure is similar, with more pronounced holes due to the formation and growth of solvent-rich regions.

When the weight ratio of diglyme to water is decreased to 4:1, the effects of spinodal decomposition become evident (Fig. 3c). Although the structure still contains a web of NOA81 and voids created by the formation of solvent-rich regions, the NOA81 web features partially formed droplets with an average size of 390 nm, as determined by image feature measurement of 50 randomly selected droplets. Interestingly, optical microscopy of the wet system just after phase separation indicated an apparent web-like structure. Subsequent evaporation of the solvent could compact such a structure to produce the morphology seen in Fig. 3c.

In Fig. 3d (diglyme to water ratio 3:1), the effects of spinodal decomposition clearly dominate. Image analysis revealed that the droplets formed are slightly larger (430 nm) and more polydisperse than those seen in Fig. 3c. Comparisons of the image features in Fig. 3c and d, along with the time to cloudiness values noted in Table 1 thus indicate a slow growth rate for the structures formed when spinodal decomposition dominates, a characteristic shared with many other morphologies formed via reaction-induced phase separation [7].

To check the effects of film thickness on structure formation and obtain images more suitable for Fourier transformation, thin films containing 5.5 wt% NOA81 in solvent consisting of diglyme and water at a 4:1 weight ratio were photocured and examined using atomic force microscopy (AFM), as shown in Fig. 4. The height image (Fig. 4a) confirms that the droplets are arranged into loosely spaced strands, while the phase image (Fig. 4b) reveals the presence of interconnecting material. The phase image is also suitable for Fourier transformation. Fig. 5 shows the one-dimensional Fast Fourier Transform (FFT) of Fig. 4b, plotted as a function of wavenumber ($2\pi/\lambda$, where λ is the feature wavelength). The peak visible in Fig. 5 corresponds to a wavelength of 370 nm.

Further insight into the mechanisms of morphology development was gained by comparing the morphologies formed by NOA65 and NOA81 in identical systems. Fig. 6 shows the SEM images for NOA65 formed in a solvent diglyme and water at a 4:1

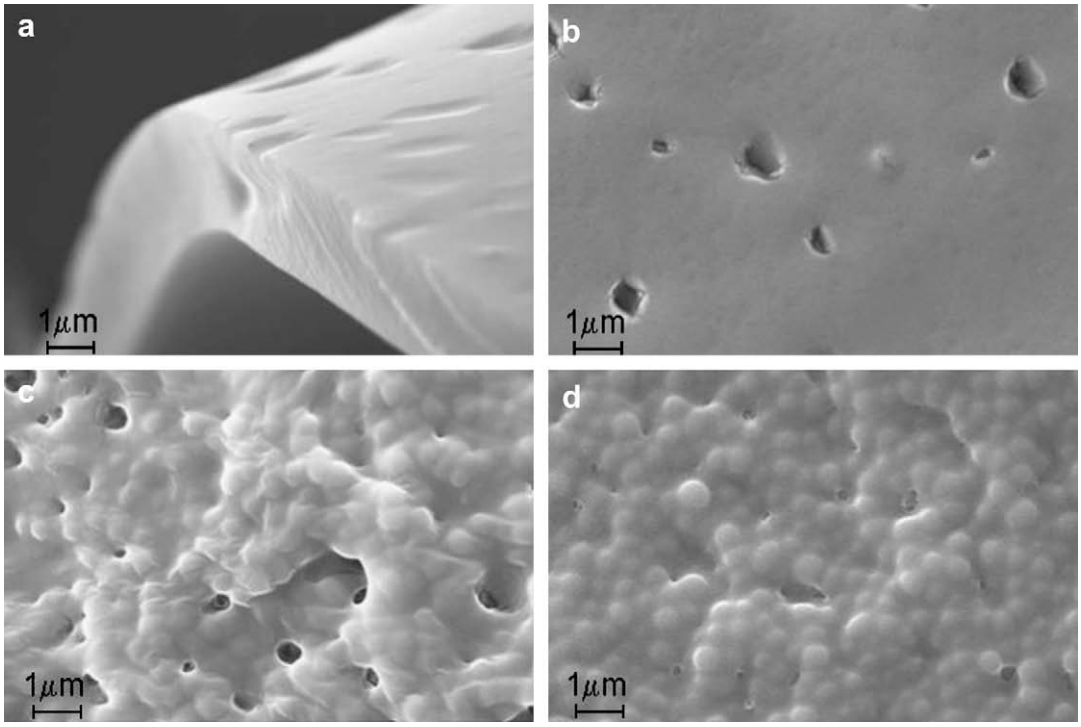

Fig. 3. SEM of phase separated morphologies produced from photopolymerization of mixtures of 5.5 wt% NOA81 dissolved in diglyme and water with diglyme to water ratios of (a) 8:1, (b) 5:1, (c) 4:1, and (d) 3:1.

weight ratio (Fig. 3c shows the analogous NOA81 system). For these systems, cloudiness was observed after 90 s of UV illumination for NOA65 as compared to 15 s for NOA81. Based on the similarity in the cloud point measurements, it is reasonable to expect that in both NOA65 and NOA81 systems, the degree of polymerization at the onset of phase separation is similar. Interestingly, the degree of interconnectedness is somewhat less with NOA65 while the average droplet size is much larger, at 1.5 μm. The polydispersity, however, remains low. Thus, although spinodal decomposition dominates the pattern formation process in both cases, the selected wavelength is much larger for NOA65.

These observations may be explained by considering the effect of quench depth (ΔT) on the selected wavelength (Λ) during spinodal decomposition, namely [7]

$$\Lambda \approx 2\pi l(3\Delta T/T_s)^{-1/2} \quad (1)$$

where T_s is the spinodal temperature and l the interaction length (on the order of 10 nm for polymer systems). As the system cures, the quench depth increases with time. For faster curing systems, the quench depth will increase more rapidly, thus, in the finite time required for droplet formation, a greater quench depth will be realized in the faster curing system, leading to a smaller selected wavelength.

Table 1
Compositions and observed phase separation onset times for NOA/water/diglyme mixtures.

Adhesive used	Composition (wt%)			Onset time (seconds)	Image
	Adhesive	Water	Diglyme		
NOA81	5.5 ± 0.1	10.5 ± 0.1	84 ± 0.1	40 ± 5	Fig. 3a
NOA81	5.5	15.8	78.8	30	Fig. 3b
NOA81	5.5	18.9	75.6	15	Figs. 3c and 4
NOA81	5.5	23.6	70.9	10	Fig. 3d
NOA65	5.5	18.9	75.6	90	Figs. 6a and 7

To facilitate further comparisons, samples of NOA65 photocured in diglyme and water at a 4:1 weight ratio were analyzed via AFM, resulting in the images shown in Fig. 7 (the analogous NOA81 images are shown in Fig. 4). The phase image (Fig. 7b) shows clearly the formation of distinct droplets. The FFT of the image in Fig. 7b is depicted in Fig. 8, which shows a peak value near the wavenumber corresponding to 1.0 μm.

The images and data shown in Figs. 3–7 clearly illustrate that viscoelastic phase separation can have an important effect on morphology development in rapidly photocured polymer/solvent mixtures, which have received relatively little attention [33] compared to the more slowly developing morphologies found in thermoplastic/thermosetting polymer mixtures or the more complicated thermoset/liquid crystal mixtures [16–18,23–25]. In fact, these results show that it is relatively simple to systematically design the morphology in these systems over a broad range of feature sizes and degree of interconnectedness. The only drawback to these systems is the significant amount of collapse that takes place on drying, which limits the ability to produce three-dimensional structures.

3.2. PIPS in mixtures of thiol-ene and low boiling solvents

As stated in Section 1, sparse network morphologies are of great technological interest because they allow for co-continuous structures to form even when the volume fraction of one of the components is quite low. The images in Figs. 3 and 4 suggest that the morphology of the UV-cured and dried optical adhesive/solvent system can resemble a loose web of filaments, consisting of individual "string of pearl" arrangements of polymer droplets. Such a morphology offers promise for the formation of sparse networks. In Figs. 3c and 4, the volume fraction occupied by polymer has increased significantly due to the collapse of the film after solvent evaporation. If the collapse can be prevented, then the formation of truly sparse networks (like those observed in mixtures of optical adhesive and liquid crystals [17]) should be possible.

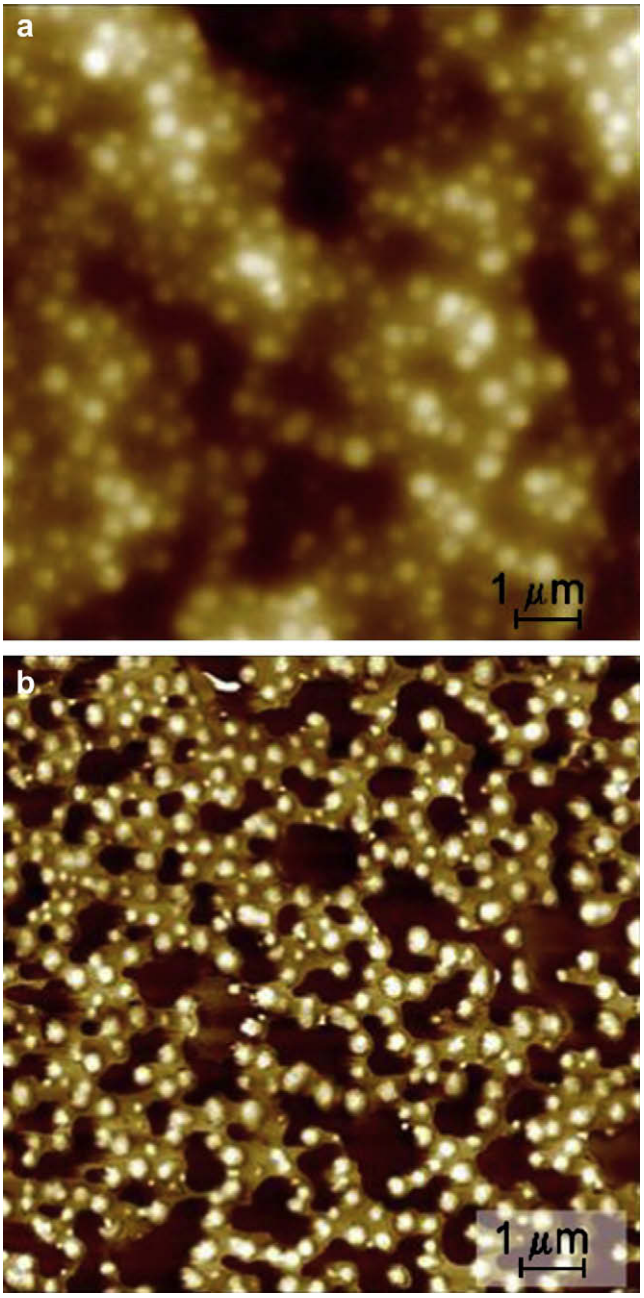

Fig. 4. Tapping mode AFM height (a) and phase (b) images of phase separated morphology produced from photopolymerization of a thin film of 5 wt% NOA81 dissolved in diglyme/water at a ratio of 4:1.

In order to minimize the opportunities for the collapse of the photocured structure in the wet film, we investigated the use of solvents with a low boiling point. We chose mixed co-solvents composed of acetone (a good solvent for the optical adhesive) and isopropanol (a non-solvent) in order to retain a means of adjusting the network morphology through changes in solvent quality, similar to the approach used in the diglyme/water systems. Our goal was to allow enough time prior to drying for the initial photocuring and phase separation to take place, then to accelerate the solidification of any sparse network by removing the solvent immediately afterward.

In order to successfully form phase separated structures in this manner, we found that a few modifications of the analogous procedure for high-boiling solvents were necessary. First, we added

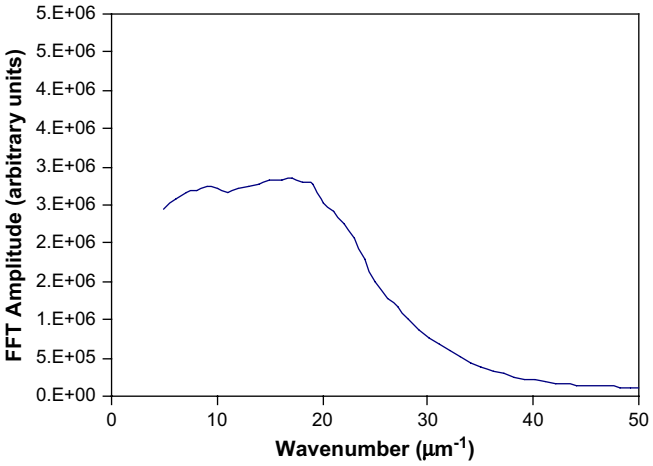

Fig. 5. One-dimensional Fast Fourier Transform of Fig. 4b.

a thermal post-cure step (1.25 min at 100 °C) immediately after the photopolymerization, to quickly remove any remaining solvent. Second, we observed that the rapid evaporation of the low viscosity solvents could lead to lateral shrinkage and surface instabilities in the films during or after casting. To overcome these difficulties, we substituted 2.5 wt% of the acetone with a polyethylene glycol (PEG) to increase the casting solution viscosity, and we increased the initial adhesive concentration to 10.0 wt%. Although previous studies of phase separation in systems containing both PEG and thiol-ene optical adhesive (albeit at much higher PEG concentrations) [34] showed evidence of PEG ordering, we could find no evidence of PEG crystallinity in the dried films using polarized optical microscopy, differential scanning calorimetry, and X-ray diffraction. We also utilized FT-IR spectroscopy to verify that the complete removal of PEG from the films was accomplished by immersing the phase separated films in water for 5 min.

Although the modified procedure remains practical for large-scale production, it introduces numerous complications into the analysis of the system. Thus, rather than attempt to create a thermodynamic model for these mixtures, we used our results from the high-boiling systems as a guide. We observed that photopolymerization of NOA81 rapidly drove the system into an unstable state, leading to phase separation in about 20 s (the compositions and times to the onset of cloudiness are listed in Table 2).

The morphologies observed on photopolymerization of the systems are shown in Fig. 9, with the amount of isopropanol in the

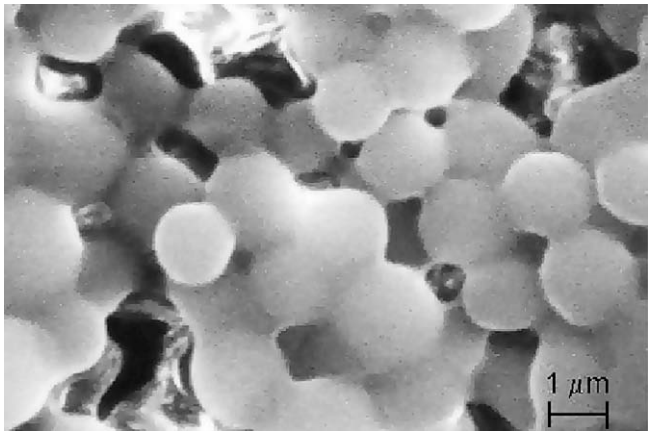

Fig. 6. SEM of phase separated morphology produced from photopolymerization of 5.5 wt% NOA65 dissolved in diglyme/water at a ratio of 4:1.

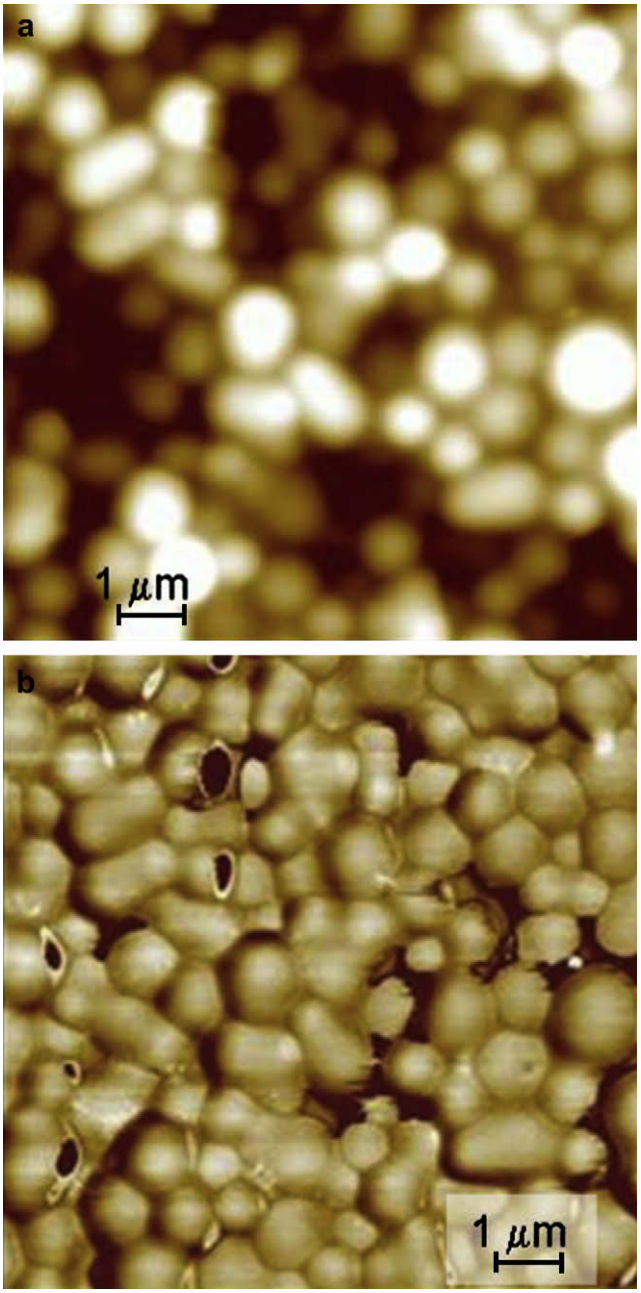

Fig. 7. Tapping mode AFM height (a) and phase (b) images of phase separated morphology produced from photopolymerization of a thin film of 5.5 wt% NOA65 dissolved in diglyme/water at a ratio of 4:1.

casting mixture varying from 15 wt% (Fig. 9a) to 30 wt% (Fig. 9b) to 40 wt% (Fig. 9c). In all cases, the feature sizes were much larger than when the high-boiling solvents are used. Fig. 9a shows a broad distribution of droplet sizes and no interconnection. In contrast, Fig. 9c shows a more uniform, interconnected structure reminiscent of spinodal decomposition, but with flattening of the domains. Fig. 9b appears to show a hybrid morphology, with a background of interconnected small droplets below a few very large interconnected droplets, creating an interesting three-dimensional structure.

The gradient of morphology seen in Fig. 9b suggests that the rapid evaporation of solvent plays a key role in the phase separation process. Even though solubility tests with pure acetone and isopropanol showed clearly that acetone is the better solvent for NOA81, the time needed for the onset of phase separation showed

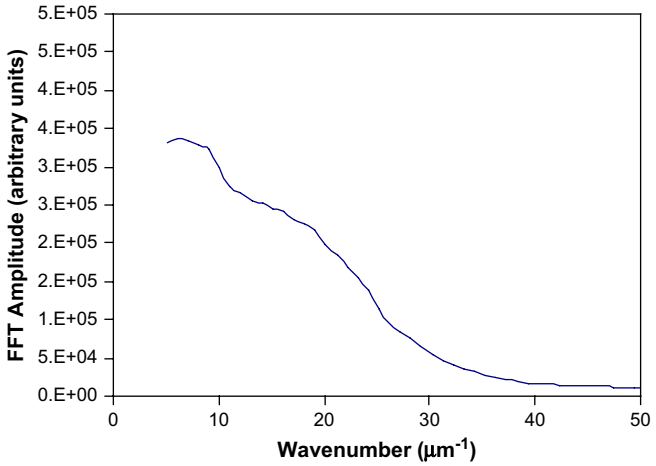

Fig. 8. One-dimensional Fast Fourier Transform of Fig. 7b.

an insignificant dependence on solvent composition. Acetone, however, evaporated at a rate two to three times faster than isopropanol under the casting conditions according to measurements taken in our laboratory. Thus, higher concentrations of acetone in the solution would have resulted in increased evaporation, leading to more rapid increases in NOA81 and isopropanol concentration, as well as to a larger degree of evaporative cooling, which would have in turn slowed down the rate of photopolymerization. These effects are expected to be most pronounced near the surface, and would have enhanced the opportunities for evaporation-induced phase separation and/or the growth and coalescence of phase separated domains prior to vitrification of the structure.

Based on the morphologies observed in Fig. 9, it thus appears that phase separation was influenced by evaporation throughout the thickness of the film when the solvent contained 15 wt% isopropanol, and in the regions of the film near the surface with 30 wt% isopropanol. In the former case, it seems that if any interconnected structures formed as a result of phase separation, the photopolymerization happened too slowly to prevent their eventual destruction. In the latter case, though, it appears that interconnected structures were preserved in at least part of the film. Interestingly, in the latter case a sparse network was formed, as the larger features that formed near the surface proved resistant to collapse and remained linked via smaller features below.

Although the results of PIPS experiments with low boiling solvents are more complex and difficult to interpret, they also illustrate the potential to realize a much broader range of morphologies by combining the effects of reaction-induced phase separation and evaporation. In particular, we have shown that the prevention of film collapse and the formation of sparse three-dimensional networks are possible by combining the effects of rapid evaporation and photopolymerization. More insight into the complicated interplay of the various phase separation dynamics in the system could be obtained through light scattering studies performed during UV irradiation, if suitable methods for protecting

Table 2
Compositions and observed phase separation onset times for NOA/acetone/isopropanol/PEG mixtures.

Adhesive used	Composition (wt%)				Onset time (seconds)	Image
	Adhesive	PEG	Acetone	Isopropanol		
NOA81	10.0 ± 0.1	1.9 ± 0.1	73.1 ± 0.1	15 ± 0.1	20 ± 5	Fig. 9a
NOA81	10.0	1.5	58.5	30	20	Fig. 9b
NOA81	10.0	1.2	48.8	40	20	Fig. 9c

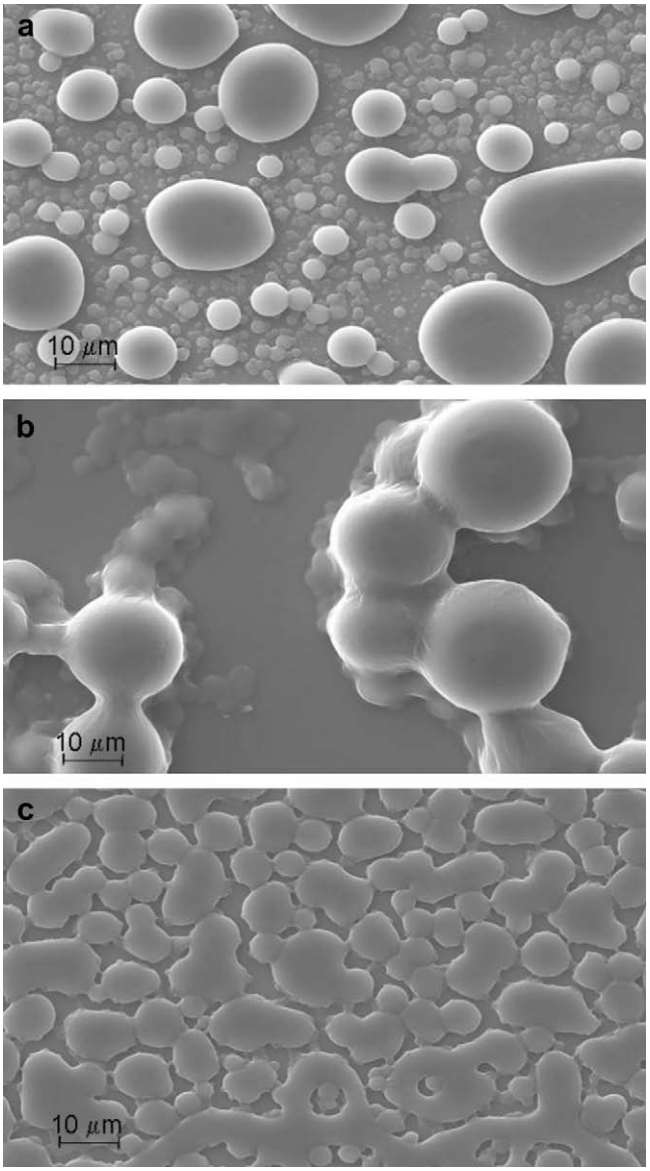

Fig. 9. SEM of phase separated morphology produced from photopolymerization of 10.0 wt% NOA81 dissolved in acetone/isopropanol/PEG, with isopropanol content of (a) 15.0 wt%, (b) 30.0 wt%, and (c) 40.0 wt%. The ratio of PEG to acetone is 2.5 wt%/97.5 wt% in all cases.

the sensitive radiation detectors involved in such experiments are available. Despite the need for more study, the experimentally observed ability to generate sparse networks using simple photocurable monomers and common solvents opens up many new and important opportunities to create advanced multi-functional polymeric materials.

4. Conclusions

Viscoelastic phase separation exhibited a strong influence on the photopolymerization-induced phase separated morphologies of polymer/solvent systems, particularly when the onset of phase separation was delayed until a high molecular weight was achieved. Using the relatively high-boiling solvents water and diglyme, we were able to produce structures with average feature sizes from 0.4 to 1.5 μm and a wide range of interconnectedness. The feature size was inversely proportional to the rate of polymerization, while the degree of interconnectedness increased as the extent of polymerization at the onset of phase separation increased. After phase separation, the phase separated structures appeared to collapse as the solvents slowly evaporated.

When the low boiling solvents acetone and isopropanol were used in the place of water and diglyme, the rapid evaporation of solvent exerted a significant influence on morphology development. When rapid evaporation took place to a larger extent, features with a larger size, a greater polydispersity, and a reduced degree of interconnectedness tended to emerge. Interestingly, when the effects of rapid evaporation were confined mainly to regions near the surface of the film, the result was the formation of a gradient morphology and the avoidance of structural collapse leading to the creation of a sparse three-dimensional network.

Acknowledgements

The authors wish to thank Mr. Dan Kline of NAWCWD for providing the SEM images, as well as the Office of Naval Research for its support. DMH wishes to thank the American Society of Engineering Education for its support through the Naval Research Laboratory Post-Doctoral Fellowship program. The software for performing Fast Fourier Transforms was kindly supplied by Dr. H.-W. Chiu.

References

[1] Hua FJ, Park TG, Lee DS. Polymer 2003;44:1911–20.
[2] Kojima J, Takenaka M, Nakayama Y, Hashimoto T. Macromolecules 2005;38:10487–93.
[3] Meng S, Duran H, Hu J, Kyu T, Natarajan LV, Tondiglia VP, et al. Macromolecules 2007;40:3190–7.
[4] Parks KL, Beckman EJ. Polym Eng Sci 1996;36:2417–31.
[5] Yamazaki M, Kayama M, Ikeda K, Alii T, Ishihara S. Carbon 2004;42:1641–9.
[6] Nishi T, Wang TT, Kwei TK. Macromolecules 1975;8:277–84.
[7] Inoue T. Prog Polym Sci 1995;20:119–53.
[8] Glotzer SC, DiMarzio EA, Muthukumar M. Phys Rev Lett 1995;74:2034–7.
[9] Murata K, Sachin J, Etori H, Anazawa T. Polymer 2002;43:2845–59.
[10] Harada A, Tran-Cong Q. Macromolecules 1997;30:1643–50.
[11] Tanaka H, Araki T. Phys Rev Lett 1997;78:4966–9.
[12] Tanaka H, Koyama T, Araki TJ. Phys Condens Matter 2005;15:5387–93.
[13] Tanaka H, Araki T. Chem Eng Sci 2006;61:2108–41.
[14] Furukawa A. J Phys Soc Jpn 2003;72:209–12.
[15] Aoki H, Kubo T, Ikegami T, Tanaka N, Hosoya K, Tokuda D, et al. J Chromatogr A 2006;1119:66–79.
[16] Kyu T, Chiu H-W. Polymer 2001;42:9173–85.
[17] Nwabumna D, Chiu H-W, Kyu T. Macromolecules 2000;33:1416–24.
[18] Amundson K, van Blaaderen A, Wiltzius P. Phys Rev E 1997;55:1646–54.
[19] Rydholm AE, Bowman CN, Anseth KS. Biomaterials 2005;26:4495–506.
[20] Bhargava R, Wang SQ, Koenig JL. Macromolecules 1999;32:8982–8.
[21] Okay O, Reddy SK, Bowman CN. Macromolecules 2005;38:4501–11.
[22] Lee TY, Roper TM, Jonsson ES, Guymon CA, Hoyle CE. Macromolecules 2004;37:3606–13.
[23] Benmouna R, Benyoucef B. J Appl Polym Sci 2008;108:4072–9.
[24] Nephew JB, Nihei TC, Carter SA. Phys Rev Lett 1998;80:3276–9.
[25] Dolgov L, Yaroshchuk O, Qiu L. Mol Cryst Liq Cryst 2007;468:335–44.
[26] Flory PJ. J Chem Phys 1942;10:51–61.
[27] Huggins ML. Ann N Y Acad Sci 1942;43:1–32.
[28] Jakob A, Grensemann H, Lohmann J, Gmehling J. Ind Eng Chem Res 2006;45:7924–33 and references therein.
[29] Brandrup J, Immergut EH. Polymer handbook. New York: John Wiley & Sons; 1989 [chapter VII].
[30] Bicerano J. Prediction of polymer properties. 3rd ed. New York: Marcel Dekker Inc.; 2002 [chapter 5].
[31] Wallace WJ, Vallenga TJ. J Chem Eng Data 1971;16:331–3.
[32] Wang X, Okada M, Han CC. Macromolecules 2006;39:5127–32.
[33] Soule E, Garcia de la Manta M, Borrajo J, Oyanguren PA, Galante MJ. J Mater Sci 2003;38:2809–14.
[34] Birnkrant MJ, McWilliams HK, Li CY, Natarajan LV, Tondiglia VP, Sutherland RL, et al. Polymer 2006;47:8147–54.